Proceedings of the International Gas Turbine Congress 2003 Tokyo
November 2-7, 2003

IGTC2003Tokyo TS-061

Second-moment turbulence closure in prediction of channel flow with system rotation

Masaaki ICHIKAWA, Shinnosuke OBI, and Shigeaki MASUDA

Department of Mechanical Engineering
Keio University
3-14-1 Hiyoshi, Kohoku-ku, Yokohama 223-8522, Japan
Phone: +81-45-563-1141 ext. 42076, FAX: +81-45-566-1495
E-mail: masaaki-ichikawa@mmm-keio.net

ABSTRACT

The assessment and improvement of a second-moment turbulence closure model is considered in predicting the fully developed turbulent channel flow rotating about the channel span. The computations are undertaken for *Re*=5000 and 5800, while the channel rotation speed ranging for $0 \leq Ro \leq 1.5$, with *Ro* being the rotation number. The detailed comparison with available DNS data is made in terms of the budget of individual Reynolds stress components. It is indicated that the system rotation causes the increase in anisotropy of dissipation rate tensor, where the dissipation rate of spanwise normal stress component, ϵ_{33}, is diminished, instead of the wall-normal component ϵ_{22} that is otherwise the smallest among the diagonal components. An improvement to the existing model has been proposed, where ϵ_{33} is damped according to the increasing rotation number. The agreement with the DNS up to *Ro*=1.5 has been achieved.

NOMENCLATURE

A	Flatness factor of a_{ij} $(= 1 - 8/9(A_2 - A_3))$
A_2	Second invariants of $a_{ij} (= a_{ij}a_{ji})$
A_3	Third invariants of $a_{ij} (= a_{ij}a_{jk}a_{ki})$
a_{ij}	Anisotropy tensor of Reynolds stress
C_{ij}	Coriolis term in $\overline{u_iu_j}$-equation
d	Half width of channel
k	Turbulent kinetic energy$(= \overline{u_iu_i}/2)$
P	Mean pressure
P^*	Reduced pressure $(= P - \rho\Omega^2 r^2/2)$
P_{ij}	Production rate of $\overline{u_iu_j}$
P_k	Production of k
Re	Reynolds number $(= 2U_m d/\nu)$
Re_t	Turbulent Reynolds number$(= k^2/\nu\epsilon)$
Ro	Rotation number $(= 2\Omega d/U_m)$
$Ro(y)$	Local Rosby number$(= -(dU/dy)/2\Omega)$
T_{ij}	Turbulent diffusion of $\overline{u_iu_j}$
U_i	Mean velocity component
U_m	Bulk mean velocity
u_i	Fluctuating velocity component
u_τ	Friction velocity
$\overline{u_iu_j}$	Reynolds stress
V_{ij}	Viscous diffusion of $\overline{u_iu_j}$
x_i	Rotating coordinate system

Greeks

δ_{ij}	Kronecker's delta
ϵ	Dissipation rate of k
ϵ_{ij}	Dissipation rate of $\overline{u_iu_j}$
ϵ_{ijk}	Eddington's tensor
ϕ_{ij}	Redistribution of $\overline{u_iu_j}$
ν	Kinematic viscosity
Ω_i	Angular velocity of system rotation
ρ	Fluid density

Subscripts

$(\ \ )$	Time averaged quantities
$(\ \ )'$	Quantities on rotating system

Manuscript Received on April 9, 2003

INTRODUCTION

The pioneering experimental investigation of rotating turbulent duct flows by Hill and Moon (1962), Moon (1964), and Moore (1967) demonstrated the action of the Coriolis forces on the mean flow and indicated a rotation-induced alteration in the turbulence field. The flow visualizations and more detailed measurements by Johnston et al. (1972) and Johnston (1973) revealed that the turbulence level in their rotating water channel was enhanced along the pressure (leading) side and was correspondingly reduced along the suction (trailing) side of the channel. They also observed the development of large-scale Taylor-Görtler-like vortices on the pressure side of the channel, while a nearly total suppression of turbulence was observed along the suction side. This re-laminarization occurred for the lower Reynolds number at relatively high rotation rates. Similar rotation-induced effects on developing turbulent boundary layers were also identified by Koyama et al. (1979). The alternation of flow field affects heat transfer characteristics as well. In addition, centrifugal buoyancy force was found to enhance heat transfer on both sides (Willet and Bergles, 2002 and Yamawaki et al., 2002).

The above-mentioned experiments have aimed at rather fundamental studies on rotation-induced flows, and the direct

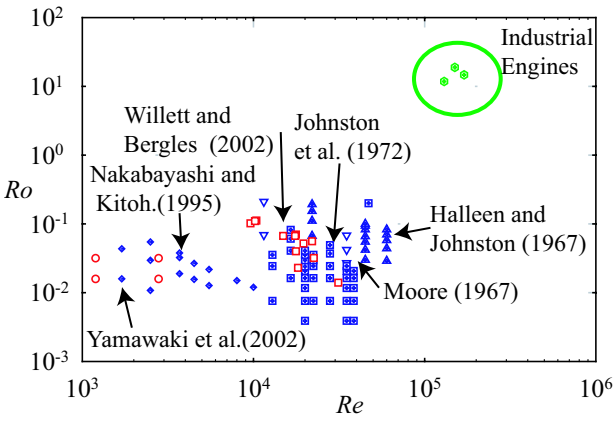

Fig.1: The comparison between the parameters tested in previous studies and industrial engines

application to engineering relevant problem is not feasible. Figure 1 summarizes the condition of experimental studies in the past in terms of Reynolds number *Re*, based on the bulk mean velocity U_m and the channel width $2d$, and rotation number *Ro*, defined by $Ro=2d\Omega/U_m$, that represents the ratio of Coriolis force and inertia force, with Ω being the rate of system rotation. The highest *Ro* that has been tested in previous studies is 0.1; comparing to the condition of industrial gas turbines which operate at *Ro*=10 or higher, there are discrepancies in two orders of magnitude. This remarkable discrepancy is attributable to technical limitation in experiments, and it is unlikely that fundamental laboratory experiments will be extended to the realistic condition in the near future.

On the other hand, the progress in high performance computers has made it possible to perform numerical simulations under the condition closer to engineering interest. To make the effects of Coriolis forces clear, direct numerical simulation (DNS) and large-eddy simulation (LES) of rotating channel flow have been undertaken in several studies. Kristofferssen and Andersson (1993) carried out DNS of rotating channel flow at *Re*=5800 and $Ro \leq 0.5$. They reported alternation in mean velocity profiles, Reynolds stresses and wall shear stress due to Coriolis force; they also reproduced secondary flow pattern similar to Taylor-Görtler vortices. Later, the budget of Reynolds stress transport equations are reported by Andersson and Kristofferssen (1995). More recently, Lamballais et al. (1996) and Lamballais et al. (1998) computed rotating channel flow at *Re*=5000 and $Ro \leq 1.5$ by means of DNS and at *Re*=14000 and $Ro \leq 1.5$ by LES. To the present authors' knowledge, their study takes up the highest *Ro* among those found in literature.

For engineering applications, computations based on Reynolds-averaged Navier-Stokes (RANS) equation are still the most feasible approach, and taking into account extreme difficulties for LES to resolve thin boundary layers at high *Re*, it is likely that the RANS models persist as the best engineering tool for next decades. Above all, eddy viscosity turbulence models, typically based on two turbulence parameters, are most popular and adopted in every commercial code. The problem in these models is that they are not able to represent the direct influence of Coriolis force on turbulent quantities because it does not appear in the transport equation of

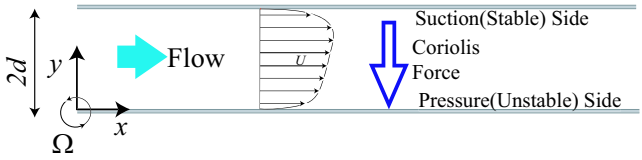

Fig.2: Schematics of the rotating channel.

turbulent kinetic energy. Hence, there are numerous studies where extension of anisotropic eddy viscosity model to rotating flow is investigated. Recent study by Nagano and Hattori (2002) proposed an anisotropic k-ϵ model with modified model transport equation for dissipation rate, and showed possibility of prediction of rotating flow by eddy viscosity models.

The present authors' opinion is, however, that the second-moment closure is straightforward and more appropriate approach to turbulence with rotation than extension of eddy viscosity models, since the effect of rotation is at least partly treated in its exact form in the transport equation of individual Reynolds stress. Admittedly, second-moment closures require more computational efforts compared to eddy viscosity models due to numerically unstable characteristics of the equation system (Obi et al., 1991), and there are still ambiguous features even in the state-of-the-art modeling strategies. Nevertheless, it is evident that the second-moment closures are capable of taking into account various physics relevant to engineering problems. The aim of the present study is, therefore, to develop a second-moment closure model that is applicable to turbulent flow with system rotation at high speed. To this end, computations are performed for fully developed channel flow so that detailed comparisons with available DNS are possible. The discussion on the possibility of new model for dissipation tensor of Reynolds stress transport equations is considered.

COMPUTATION

Governing Equations

Fully developed turbulent flow between two infinite parallel walls rotating around the span-wise axis is considered, cf. Fig. 2. The walls are named pressure (unstable) or suction (stable) side, respectively, according to customary. The resulting flow, which is assumed to be incompressible, is characterized by the following mean streamwise momentum equation:

$$0 = -\frac{1}{\rho}\frac{\partial P^*}{\partial x} - \frac{d}{dy}\overline{uv} + \nu\frac{d^2U}{dy^2} \qquad (1)$$

In the above equation, the gradient of reduced pressure $P^* = P - \rho\Omega^2 r^2$is uniform in entire flow field. Also, Eq. (1) shows that the total shear stress varies linearly across the channel as in non-rotating flow.

The exact equation governing Reynolds stress transport can be written as

$$\frac{D\overline{u_i u_j}}{Dt} = P_{ij} + C_{ij} + V_{ij} + T_{ij} + \phi_{ij} - \epsilon_{ij} \qquad (2)$$

with

$$P_{ij} = -\left(\overline{u_k u_i}\frac{\partial U_j}{\partial x_k} + \overline{u_k u_j}\frac{\partial U_i}{\partial x_k}\right),$$

$$C_{ij} = -2\left(\epsilon_{ikl}\Omega_k\overline{u_l u_j} + \epsilon_{jkl}\Omega_k\overline{u_l u_i}\right),$$

$$V_{ij} = \frac{\partial}{\partial x_k}\left(\nu\frac{\partial\overline{u_i u_j}}{\partial x_k}\right),$$

$$T_{ij} = -\frac{\partial}{\partial x_k}\left[\overline{u_k u_i u_j} + \frac{1}{\rho}\overline{p\left(u_j\delta_{ik} + u_i\delta_{jk}\right)}\right],$$

$$\phi_{ij} = \overline{\frac{p}{\rho}\left(\frac{\partial u_i}{\partial x_j} + \frac{\partial u_j}{\partial x_i}\right)},$$

$$\epsilon_{ij} = 2\nu\overline{\frac{\partial u_i}{\partial x_k}\frac{\partial u_j}{\partial x_k}},$$

where the over-bar indicates the quantities after ensemble averaging. The terms P_{ij}, C_{ij}, V_{ij}, T_{ij}, ϕ_{ij} and ϵ_{ij} are identified as production, Coriolis production, viscous diffusion, turbulent diffusion including the pressure diffusion, redistribution, and dissipation of $\overline{u_i u_j}$. Among them, P_{ij}, C_{ij} and V_{ij} are treated in exact form while the others need to be modeled.

Turbulence Model

In this work, the model developed by Launder and Shima (1989) has been selected because it predicts a variety of flows fairly well despite that its relatively simple formulation (Jakirlić, 1997). The model formulation is briefly reviewed.

For the turbulent diffusion, the generic gradient diffusion model of Daly and Harlow (1970) is adopted:

$$T_{ij} = -\frac{\partial}{\partial x_k}\left(C_s\frac{k}{\epsilon}\overline{u_k u_m}\frac{\partial\overline{u_i u_j}}{\partial x_m}\right). \tag{3}$$

The sum of the dissipation and redistribution terms is expressed as:

$$\begin{aligned} -\epsilon_{ij} + \phi_{ij} &= -\frac{2}{3}\epsilon\delta_{ij} + \phi_{(1)ij} + \phi_{(2)ij} + \phi_{(3)ij} \\ &\quad + \phi^w_{(1)ij} + \phi^w_{(2)ij} + \phi^w_{(3)ij} \end{aligned} \tag{4}$$

where $\phi_{(1)ij}$is the slow redistribution term including the anisotropic part of dissipation, $\phi_{(2)ij}$ is the rapid part, and $\phi_{(3)ij}$ is the redistribution term due to Coriolis production. $\phi^w_{(1)ij}$, $\phi^w_{(2)ij}$ and $\phi^w_{(3)ij}$ are wall reflection terms of redistribution terms respectively. For these redistribution terms, the following models are adopted:

$$\phi_{(1)ij} = -C_1^*\epsilon a_{ij}, \tag{5}$$

$$\phi_{(2)ij} = -C_2^*\left(P_{ij} - \frac{2}{3}\delta_{ij}P_k\right), \tag{6}$$

$$\phi_{(3)ij} = -\frac{1}{2}C_2^* C_{ij}, \tag{7}$$

where a_{ij} in Eq. (5) is the anisotropy tensor of Reynolds stress ($a_{ij} = \overline{u_i u_j} - 2/3k\delta_{ij}$), and P_k in Eq. (6) is the production rate of k, ($P_k = P_{ii}/2$).

Table 1: Model Constants

C_1	C_2	C_1'	C_2'	C_s	C_l	$C_{\epsilon 1}$	$C_{\epsilon 2}$	C_ϵ
2.58	0.75	1.67	0.50	0.22	2.5	1.45	1.9	0.18

Wall proximity effects on the redistribution process are represented by additional terms written as:

$$\begin{aligned} \phi^w_{(1)ij} &= -C_1^*\frac{\epsilon}{k}\left(\overline{u_k u_m}n_k n_m\delta_{ij} - \frac{3}{2}\overline{u_k u_i}n_k n_j \right. \\ &\quad \left. -\frac{3}{2}\overline{u_k u_j}n_k n_i\right) f_w \end{aligned} \tag{8}$$

$$\begin{aligned} \phi^w_{(2)ij} &= \frac{C_2'^*}{C_2^*}\left(\phi_{(2)km}n_k n_m\delta_{ij} - \frac{3}{2}\phi_{(2)ik}n_k n_j \right. \\ &\quad \left. -\frac{3}{2}\phi_{(2)jk}n_k n_i\right) f_w \end{aligned} \tag{9}$$

$$\begin{aligned} \phi^w_{(3)ij} &= \frac{C_2'^*}{C_2^*}\left(\phi_{(3)km}n_k n_m\delta_{ij} - \frac{3}{2}\phi_{(3)ik}n_k n_j \right. \\ &\quad \left. -\frac{3}{2}\phi_{(3)jk}n_k n_i\right) f_w \end{aligned} \tag{10}$$

where f_w is an empirical function to control the wall proximity effect, which appears in the present study as:

$$f_w = \frac{k^{3/2}}{\epsilon C_l}\left(\frac{1}{y} + \frac{1}{2d-y}\right). \tag{11}$$

The model coefficients are determined by:

$$C_1^* = 1 + C_1\left\{1 - \exp\left[-\left(0.0067Re_t\right)^2\right]\right\}AA_2^{1/4} \tag{12}$$

$$C_2^* = C_2 A^{1/2} \tag{13}$$

$$C_1'^* = -2C_1^*/3 + C_1^* \tag{14}$$

$$C_2'^* = \left[2\left(C_2^* - 1\right)/3 + C_2^* + \left|\left(C_2^* - 1\right)/3 + C_2^*\right|\right]/2 \tag{15}$$

The dissipation rate of turbulent kinetic energy ϵ, appearing in Eq. (4), is computed by the following transport equation:

$$\begin{aligned} \frac{D\epsilon}{Dt} &= \left(C_{\epsilon 1} + \psi_1 + \psi_2\right)\frac{\epsilon}{k}P_k - C_{\epsilon 2}\frac{\epsilon\tilde{\epsilon}}{k} \\ &\quad + \frac{\partial}{\partial x_m}\left(C_\epsilon\frac{k}{\epsilon}\overline{u_m u_l}\frac{\partial\epsilon}{\partial x_l} + \nu\frac{\partial\epsilon}{\partial x_m}\right), \end{aligned} \tag{16}$$

where

$$\tilde{\epsilon} = \epsilon - 2\nu\left(\frac{\partial\sqrt{k}}{\partial x_l}\right)^2. \tag{17}$$

The functions ψ_1 and ψ_2 in Eq. (16) are defined as:

$$\psi_1 = 1.5A\left(P_k/\epsilon - 1\right), \tag{18}$$

$$\psi_2 = 0.35\exp\left[-\left(0.002Re_t\right)^{1/2}\right]\left(1 - 0.3A_2\right). \tag{19}$$

ψ_1 has the effect to reduce turbulence length scale, and ψ_2 controls re-laminarization of turbulent flow under favorable

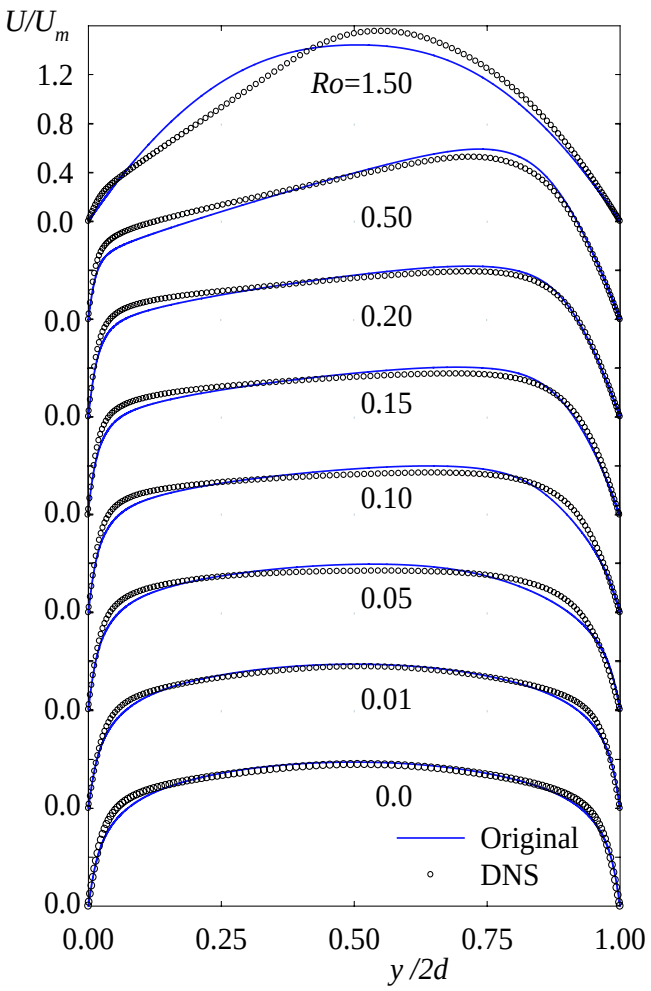

Fig.3: Mean velocity profile for *Re*=5800, *Ro*=0∼0.50 and *Re*=5000, *Ro*=1.50

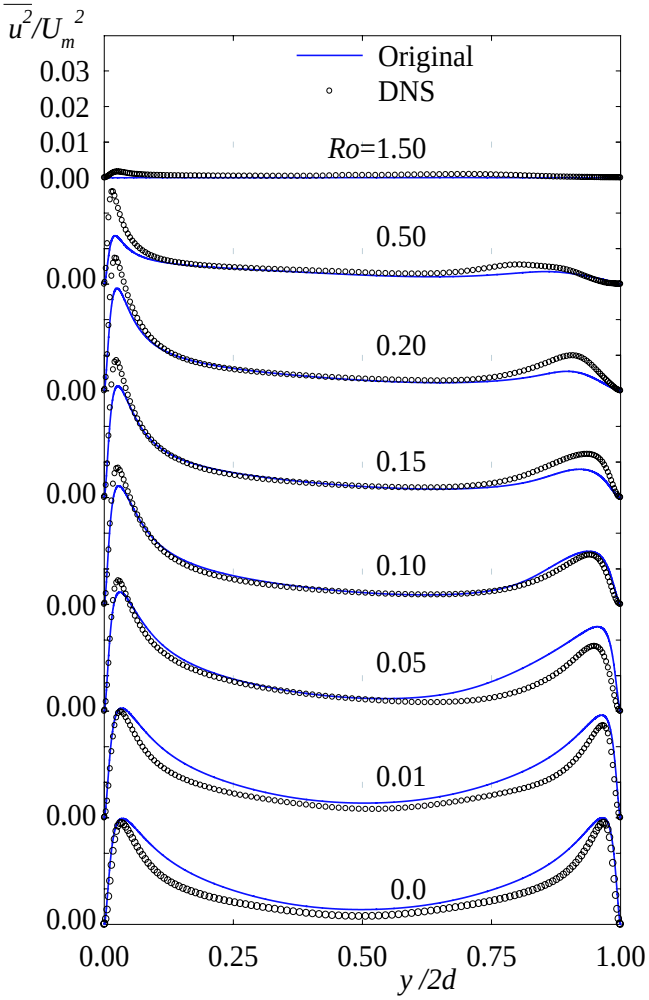

Fig.4: Reynolds Stress $\overline{u^2}$ for *Re*=5800, *Ro*=0∼0.50 and *Re*=5000, *Ro*=1.50

pressure gradient. The values of the model constants used in this study are summarized in Table 1.

Numerical Method

The above equations were solved by finite volume method with collocated grid arrangement (Obi et al., 1991, Jakirlić, 1997). Rectangular grids were used, which comprised non-equidistantly distributed 200 control volumes in the y-direction. The distance between the wall and nearest node was determined to be $y^+ = yu_\tau/\nu \approx 0.1$, and the distance between each node was increased in a geometric progression with an expansion ratio of about 1.05. On the solid wall, Reynolds stress and the mean velocity were set to 0, while a finite value was assigned to the dissipation rate as $\epsilon = 2\nu \left(\partial\sqrt{k}/\partial x_l\right)^2$, which represents the exact limit.

RESULTS AND DISCUSSION

Computation by Original Model

Results of computations for rotating channel flows are presented for Reynolds number *Re*=5000 and 5800, based on the bulk mean velocity U_m and the channel width $2d$, in order to compare with the data of DNS by Kristofferssen and Andersson (1993) and Lamballais et al. (1998). For this application, different values of the rotation number $Ro=2d\Omega/U_m$ are considered, which corresponds to $0 \leq Ro \leq 0.5$ at *Re*=5800 and *Ro*=1.5 at *Re*=5000.

Figure 3 compares the mean velocity predicted by the original model and those from the corresponding DNS. The vertical axis is normalized by the bulk mean velocity U_m and the horizontal axis by the channel width $2d$. The left- and right-hand sides of the graph correspond to the pressure- and the suction-side, respectively. The result by DNS indicates that the velocity profile becomes gradually asymmetric about the center of the channel as the rotation rate increases. The computations by the original model represent this trend fairly well up to *Ro*∼0.5. However, the model fails to predict the asymmetric profile of DNS at the highest rotation number, *Ro*=1.5, yielding a velocity distribution similar to parabolic laminar one.

The three normal components of Reynolds stress, $\overline{u^2}$, $\overline{v^2}$, $\overline{w^2}$ and the shear stress $\overline{uv}$ are presented in Figs. 4 to 7 at the same condition as for the mean velocity profile in Fig. 3. The overall tendency shown by the results of DNS is that the Reynolds stresses are reduced on the suction side and increased on the pressure side as a result of the imposed system rotation. The computation by second-moment closure shows the similar tendency as DNS for $0 \leq Ro \leq 0.5$. However, as was the case in the mean velocity profile, the agreement with DNS becomes worse at the highest *Ro* shown here. All Reynolds stress components nearly disappear at *Ro*=1.5,

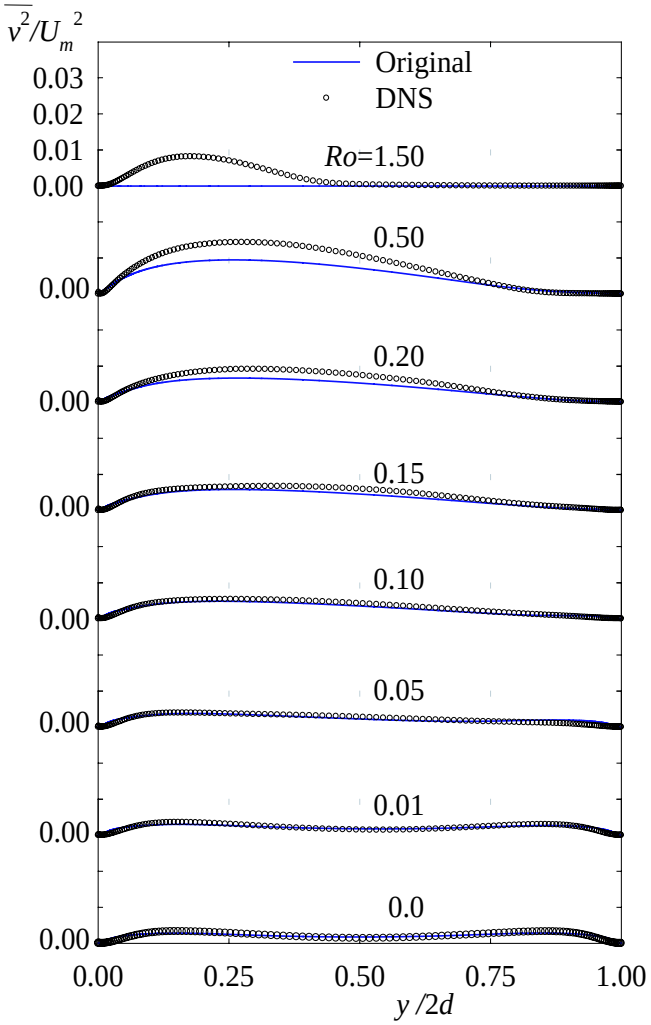

Fig.5: Reynolds Stress $\overline{v^2}$ for *Re*=5800, *Ro*=0∼0.50 and *Re*=5000, *Ro*=1.50

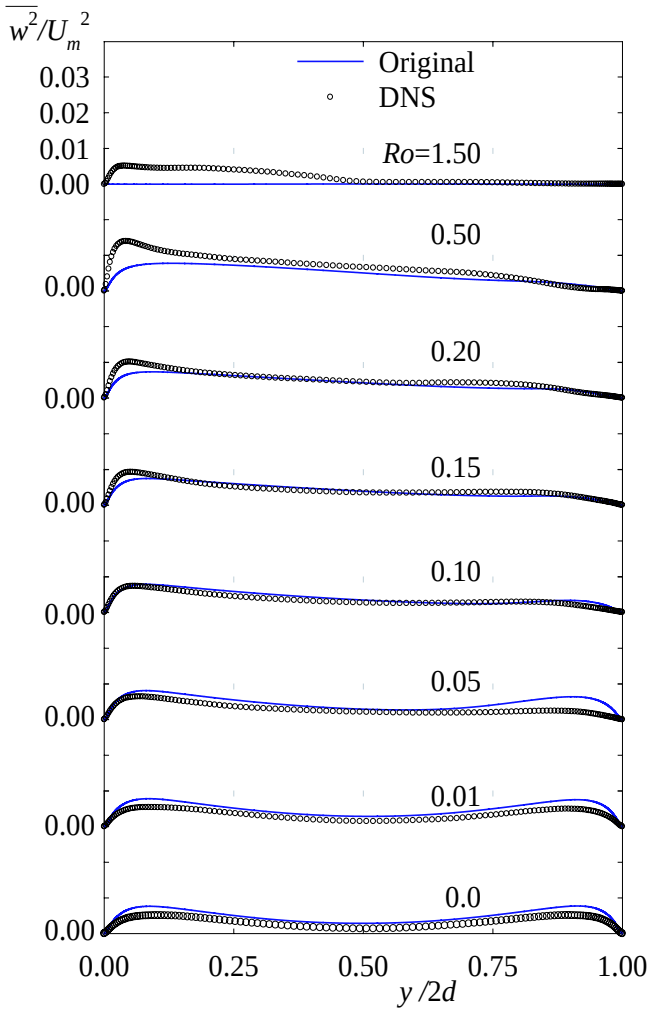

Fig.6: Reynolds Stress $\overline{w^2}$ for *Re*=5800, *Ro*=0∼0.50 and *Re*=5000, *Ro*=1.50

which corresponds to the laminar-like mean velocity profile.

Effect of System Rotation

The cause for the failure of prediction at highest rotation number is now considered. In general, it is difficult to pinpoint a part of the turbulence model which is responsible for the discrepancy, because in such a non-linear equation system any tiny alternation in a single term may result in the change in the overall result. Among some candidates, the dissipation rate tensor is scrutinized in the present study. This is in accordance with the proposal by Jongen et al. (1998) who introduced an anisotropy effect of dissipation tensor to an explicit algebraic stress model. Here, the modification is made based on more phenomenological observation.

The basis in this study is *Taylor-Proudman theorem*, namely, the flow does not change in the direction parallel to the rotation axis when the system rotates at very high rate. Since the channel rotates about the spanwise axis, the theorem can be formulated as:

$$\frac{\partial u_i}{\partial z} \simeq 0. \tag{20}$$

Owing to Eq. (20), vortex filaments in the flow field are expected to align parallel to the z-axis in the case of high rotation. It is natural to consider that this alignment occurs in every scale of turbulence, including the dissipation length scale. Hence, in the case of high rotation,

$$\epsilon_{33} < \epsilon_{11}, \epsilon_{22} \tag{21}$$

may be induced.

As mentioned in the previous section, LS model treats the dissipation term together with the slow part of redistribution process, cf. Eq. (4). The basic concept of this treatment may be interpreted as the separation of dissipation term into isotropy part and anisotropy part, namely:

$$\epsilon_{ij} = \frac{2}{3}\epsilon\delta_{ij} + \phi_{(\epsilon)ij} \tag{22}$$

The anisotropy part represents the wall proximity effects and hence persists regardless of system rotation. Therefore, to take into account the effect of system rotation, an additional anisotropy part is necessary, i.e.:

$$\epsilon_{ij} = \frac{2}{3}\epsilon\delta_{ij} + \phi_{(\epsilon)ij} + \phi^R_{(\epsilon)ij} \tag{23}$$

The third term on the right hand side represents the influence of system rotation on the individual dissipation-rate tensor component. The amplitude of $\phi^R_{(\epsilon)ij}$ is to be estimated by, e.g., using available DNS data set.

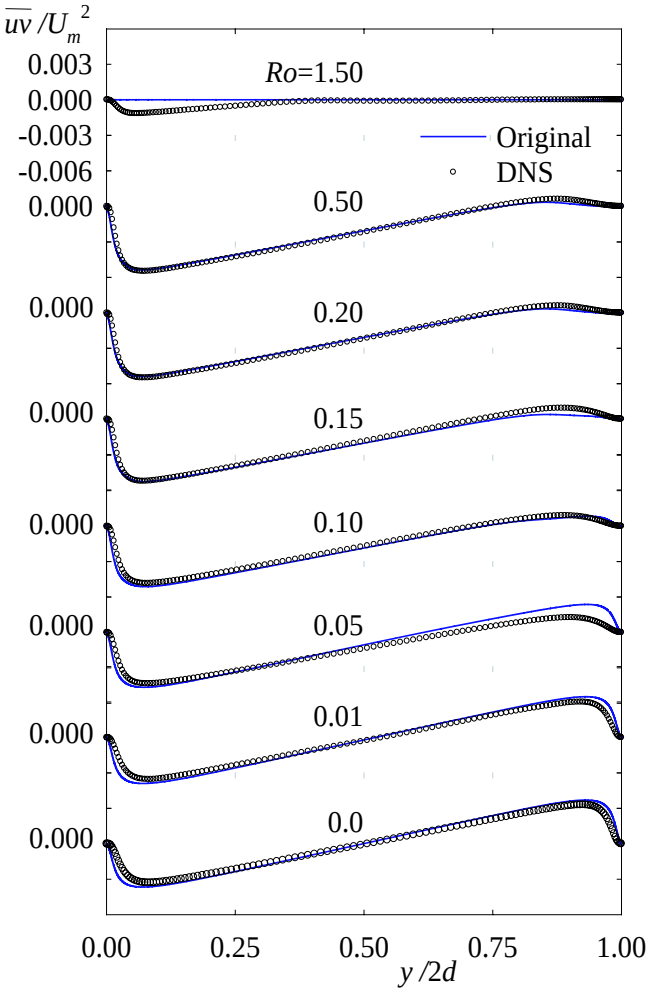

Fig.7: Reynolds Stress $\overline{uv}$ for *Re*=5800, *Ro*=0∼0.50 and *Re*=5000, *Ro*=1.50

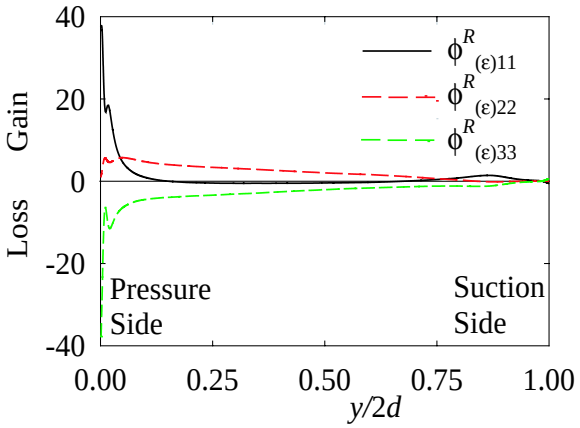

Fig.8: Anisotropy part of dissipation caused by system rotation for *Re*=5800, *Ro*=0.50

The evaluation based on DNS data of Andersson (1993) and Lamballais et al. (1996) has been undertaken as follows: First, the anisotropy part of the dissipation tensor in Eq. (22) was calculated for the case without system rotation by subtracting the isotropic part $(2/3)\epsilon\delta_{ij}$ from ϵ_{ij}. The comparison between individual components of $\phi_{(\epsilon)ij}$ indicated that there is indeed strong anisotropy in the dissipation rate tensor, with $\phi_{(\epsilon)22}$ being negative in the region close to the wall, which is explained by the wall asymptotic behavior. Second, under the system rotation, the additional anisotropy term $\phi^R_{(\epsilon)ij}$ was calculated by rearranging Eq. (23):

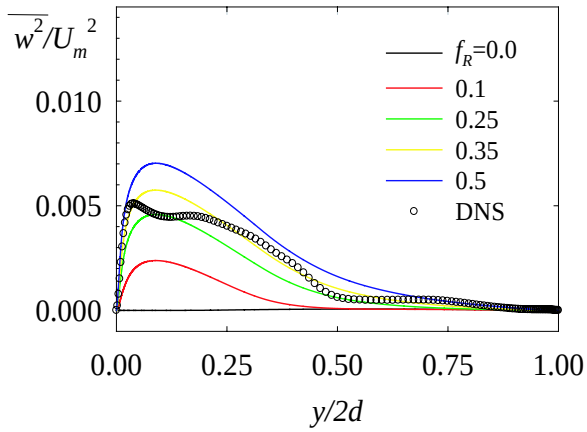

Fig.9: Optimization of the model function $f\,(Ro)$ for *Re*=5000, *Ro*=1.50

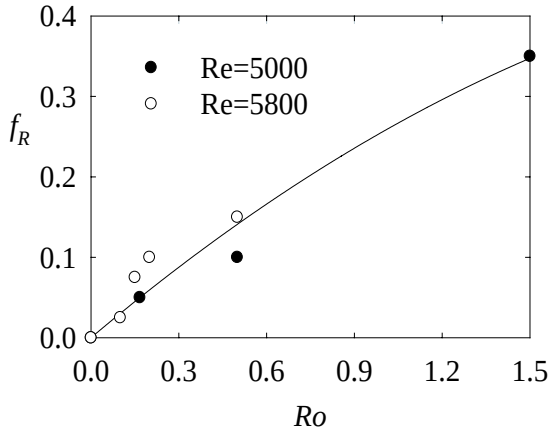

Fig.10: Determination of the model function f_R.

$$\phi^R_{(\epsilon)ij} = \epsilon'_{ij} - \frac{2}{3}\epsilon'\delta_{ij} - \epsilon'\frac{\phi_{(\epsilon)ij}}{\epsilon}. \qquad (24)$$

It should be noted that the terms on the right hand side are distinguished by $'$ from their value in stationary system. Because the two anisotropic parts in Eq. (23) can not be divided from each other at this stage, it is assumed that the ratio of the "stationary" anisotropy part to the isotropy part, $\phi_{(\epsilon)ij}/\epsilon$, stays constant regardless of the system rotation. The distribution of the individual terms is shown in Fig. 8 for the rotating case at *Ro*=0.5. As expected, $\phi^R_{(\epsilon)33}$ has negative contribution throughout the channel cross section, which supports the argument shown by Eq. (21).

Correction Based on Rotation Number

Based on the above-mentioned investigation, a modification to the dissipation tensor of Reynolds stress equation is considered. There are several choices in strategy for reducing ϵ_{33} on the rotating system. After some trials, it is found that the formation below provides satisfactory improvement

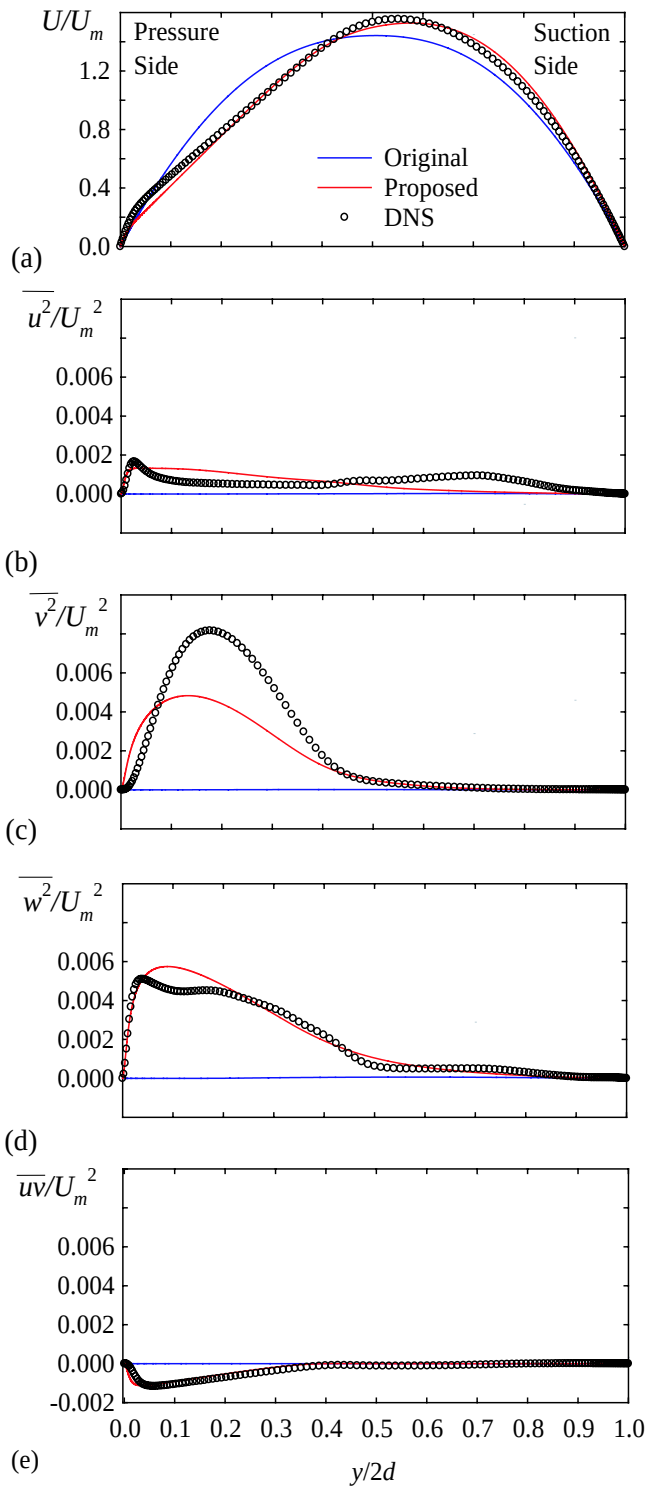

Fig.11: Prediction of mean velocity and Reynolds stress components by modified model for *Re*=5000, *Ro*=1.50. (a) Mean velocity, (b) $\overline{u^2}$, (c) $\overline{v^2}$, (d) $\overline{w^2}$, (e) $\overline{uv}$

to the original model,

$$\phi^R_{(\epsilon)ij} = -\frac{2}{3} f_R \epsilon \, \delta_{i3}\delta_{3j}, \qquad (25)$$

where f_R is a function that increases with the increasing *Ro*. It should be noted that Eq. (25) is not applicable to system rotation about an arbitrary axis, but only for the present case where the axis of rotation is parallel to z-direction. Besides, this formulation sensitizes the dissipation rate to the system rotation regardless of the local quantity like mean shear rate or vorticity.

The relationship between f_R and *Ro* has been investigated with regard to the prediction of $\overline{w^2}$ component at *Ro*=1.5 as shown in Fig. 9. Based on the comparison with DNS by Lamballais et al. (1996), the value of f_R at *Ro*=1.5 has been determined to 0.35. The analogous investigations are performed for a wider range of *Ro* and two different Reynolds numbers, and a functional relationship between f_R and *Ro* has been specified, cf. Fig. 10. The proposed form of f_R is:

$$f_R = -0.0503 Ro^2 + 0.307 Ro, \text{ for } 0 \le Ro \le 1.5. \qquad (26)$$

The computation by the proposed model formulation is performed, and the results are shown in Fig. 11. It is indicated that the agreement of the predicted mean velocity as well as the all Reynolds stress components with the DNS is remarkably improved. The present results point to the fact that a small modification to the model equation of $\overline{w^2}$-component, that has no direct effect in the two-dimensional flow, alters the shear stress component through nonlinear interaction between Reynolds stress components, and eventually changes the mean velocity profile. It should be stressed that the discussion on the model improvement has been based on a theorem which is known for long time, and not on a pure mathematical consideration such as series expansion, etc. It is also demonstrated that the second-moment closure modeling is a straightforward and simple way to incorporate various physics into the engineering flow prediction. The generalization of the proposed model should be performed at higher rotation numbers and also in more complex flow configurations.

CONCLUSION

The computations of fully developed turbulent channel flow with system rotation are performed by a second-moment turbulence closure within the RANS framework. The predictions calculated with the original Launder-Shima model show good agreement with DNS at rotation numbers of only up to 0.5. For the improvement of flow computation at higher Rotation numbers, the modification to the dissipation equation has been considered. The present study has proposed an additional term that suppresses ϵ_{33} component, i.e., the dissipation of normal stress component in the direction of rotation axis. Together with an empirical relationship on the rotation number, the prediction of fully developed channel flow at *Ro*=1.5 has been successfully performed.

ACKNOWLEDGEMENT

The authors are grateful to Professor H. I. Andersson, Norwegian University of Science and Technology, and Professor E. Lamballais, Poitiers University, for generously making the data of DNS available. Dr. S. Jakirlić, Technical University of Darmstadt, has provided the basic version of the code, which is greatly appreciated.

References

Andersson, H. I., and Kristofferssen, R., 1995 "Turbulence Statistics of Rotating Channel Flow" Turbulent Shear Flows, 9, 53-70.

Daly, B. J., and Harlow, F. H., 1970 "Transport Equations in Turbulence" Phys. Fluids 13, 2634-2649.

Hattori, H., and Nagano, Y., 2002 “An Improved Turbulence Model for Rotating Shear Flows” Trans. JSME, B68-667, 761-768 (in Japanese).

Hill, P. G., and Moon, I. M., 1962 “Effects of Coriolis on the Turbulent Boundary Layer in Rotating Fluid Machines” MIT Gas Turbine Lab. Rep. 69.

Jakirlić, S., 1997 *Reynolds-Spannungs-Modellierung komplexer turbulenter Stroömungen*, Herbert Utz Verlag Wissenshaft, Munich.

Johnston, J. P., 1973 “The Suppression of Shear Layer Turbulence in Rotating Systems” Trans. ASME I: J. Fluids Eng. 95, 229-236.

Johnston, J. P., Halleen, R. M., and Lezius, D. K., 1972 “Effects of Spanwise Rotation on the Structure of Two-dimensional Fully Developed Turbulent Channel Flow” J. Fluid Mech. 56, 533-557.

Jongen, T., Machiels, L., and Gatski, T. B., 1998 “Predicting Noninertial Effects with Linear and Nonlinear Eddy-Viscosity, and Algebraic Stress Models” Flow, Turbulence and Combustion 60, 215-234.

Koyama, H., Masuda, S., Ariga, I. and Watanabe, I., 1979 “Stabilizing and Destabilizing Effects of Coriolis Force on Two-dimensional Laminar and Turbulent Boundary Layers.” Trans. ASME A: J. Eng. Power 101, 23-31.

Kristofferssen, R., and Andersson, H. I. 1993 “Direct Simulations of Low-Reynolds-number Turbulent Flow in a Rotating Channel” J. Fluid Mech., 256, 163-197.

Lamballais, E., Lesieur, M., and Metais, O. 1996 “Effects of Spanwise Rotation on the Vorticity Stretching in Transitional and Turbulent Channel Flow” Int. J. Heat and Fluid Flow, 17, 324-332.

Lamballais, E., Lesieur, M., and Metais, O., 1998 “Spectral-Dynamic Model for Large-Eddy Simulations of Turbulent Rotating Channel Flow” Theoretical and Computational Fluid Dynamics, 12, 149-177.

Launder, B. E., and Shima, N., 1989 “Second-Moment Closure for the Near-Wall Sublayer : Development and Application” AIAA J., 27-10, 1319-1325.

Moon, I. M., 1964 “Effects of Coriolis Forces on the Turbulent Boundary Layer in Rotating Fluid Machines” MIT Gas Turbine Lab. Rep. 74.

Moore, J., 1967 “Effect of Coriolis forces on Turbulent Flow in Rotating Rectangular Channels” MIT Gas Turbine Lab. Rep. 89.

Obi, S., Perić, M., and Scheuerer, G., 1991 “Second-moment calculation procedure for turbulent flows with collocated variable arrangement” AIAA J., 29-4, 585-590.

Tritton, D. J., 1992 “Stabilization and Destabilization of Turbulent Shear Flow in a Rotating Fluid” J. Fluid Mech., 241, 503-523.

Willett, F. T., and Bergles, A. E., 2002 “Heat Transfer in Rotating Narrow Rectangular Ducts With Heated Sides Parallel to the r-z Plane” Trans. ASME, J. Heat Transfer, 124, 1-7.

Yamawaki, D., Obi, S., and Masuda, S., 2002 “Heat Transfer in Transitional and Turbulent Boundary Layers with System Rotation” Int. J. Heat and Fluid Flow, 23, 186-193.